Materials Characterization 164 (2020) 110308

Contents lists available at ScienceDirect

Materials Characterization

journal homepage: www.elsevier.com/locate/matchar

An alternative method for the measurement of precipitate volume fractions in microalloyed steels by the means of atom probe tomography

Alexis Graux[a], Sophie Cazottes[a,*], Damien Fabrègue[a], Michel Perez[a], Frédéric Danoix[b]

[a] Univ. Lyon, INSA Lyon, MATEIS, UMR CNRS 5510, F-69621 Villeurbanne, France
[b] Normandie Univ, UNIROUEN, INSA Rouen, CNRS, Groupe de Physique des Matériaux, 76000 Rouen, France

ARTICLE INFO

Keywords:
Atom probe tomography
Microalloyed steels
Precipitation
Volume fraction
Solubility product

ABSTRACT

Knowledge of the volume fraction of precipitates is crucial for estimating the impact of precipitation on microstructure evolution or mechanical properties. However, its experimental determination is often a difficult task. In this work, atom probe tomography was applied to an industrial Ti−Nb microalloyed steel, to follow the evolution of austenite solute composition in titanium and niobium as a function of temperature in the austenitic domain. These composition measurements were used to calculate the volume fraction of $(Ti_x, Nb_{1-x})C$ carbides in austenite, using mass balance. This type of measurement is made possible by the considerable evolutions experienced by tomographic atom probes over the past 20 years in terms of volume analyzed and mass resolution. Atom probe tomography is nowadays not only able to help determining volume fractions below 0.1%, but also provides unique information related to solubility limits as low as a few tens of ppm, most useful for developing phase diagrams, or assessing existing ones.

1. Introduction

In microalloyed steels, elements such as Ti and Nb form precipitates that control grain growth [1] and cause precipitation strengthening [2]. Precipitate volume fraction and precipitate radii have a key impact on the resulting mechanical properties. Grain growth and precipitate hardening are indeed both controlled by the precipitate size distribution. The precipitate size distribution is usually described by its mean radius $\langle r \rangle$ and volume fraction f_v, the determination of which is therefore critical to estimate the effect of precipitation on microstructure evolution and mechanical properties.

Transmission electron microscopy (TEM) techniques directly allow the determination of the distribution of precipitate sizes. The determination of f_v by TEM is however quite imprecise. From thin foil observations, it is difficult to measure precisely the local thickness of the foil [3], which may not be constant over the observed field of view, leading to large scatter in the observed volume of matrix. Moreover, for low volume fractions, the number of observed precipitates in a single field of view drops to values that often hinders any statistical analysis. This procedure then often turns out to be inaccurate. The estimation of volume fraction using extraction replicas [4] also imposes to estimate the etched volume of matrix, which depends on the studied material, etching time, and many other (uncontrolled) experimental factors. Other techniques are thus needed to estimate the volume fraction of precipitates.

The most common method is to resort to selective matrix dissolution techniques coupled with inductively coupled plasma (ICP) spectroscopy [5–7]. These techniques aim at isolating the precipitates present in the steel by chemical or electrolytic dissolution of the matrix. Both the precipitates isolated by filtration, and the resulting solution (dissolved matrix) are then analyzed to determine the respective proportions of elements present in precipitates and in solid solution. Selective matrix dissolution has the advantage of providing a global composition of large samples but requires a strong experience in sample preparation, etching solutions, and precipitate filtering.

Small Angle X-rays Scattering (SAXS) and Small Angle Neutron Scattering (SANS) also allow to measure precipitate volume fractions [8,9]. With these techniques, the detection limit depends on the type of precipitates. In some cases, volume fraction of approximately 0.1% can be difficult to quantity. It is also hard to distinguish different types of precipitates, having different compositions, if they present similar sizes. Last, these techniques necessitate the access to large-scale facilities.

Alternatively, atom probe field ion microscopy (APFIM) or atom probe tomography (APT) can be applied for indirect precipitate volume fraction determination through the measurement of matrix composition. These techniques have indeed already been applied to high speed steels [10] or Al-Zn-Mg alloy [11] to measure the matrix composition and derive the volume fraction of precipitates. In both studies, volume

* Corresponding author.
E-mail address: sophie.cazottes@insa-lyon.fr (S. Cazottes).

https://doi.org/10.1016/j.matchar.2020.110308
Received 13 November 2019; Received in revised form 31 March 2020; Accepted 31 March 2020
Available online 28 April 2020

fractions of precipitates were rather large (of the order of 1 to 10%), leading to low relative uncertainties. In 1994, Palmière et al. [12] applied APFIM, the 1D ancestor of current APT, to study the evolution of Nb solute content in austenite for various heat treatments in Nb-microalloyed steels. Although original and promising, this methodology was then limited by the volume sizes (and thus the number of atoms analyzed), the mass resolution of the instrument, and its one-dimensional nature. At last, the instrument they used only provided 1D concentration profiles, rather than 3D reconstruction. As a consequence, they developed a procedure to discriminate between matrix and precipitates. Their procedure can be questioned, but is no longer necessary nowadays, with true 3D atomic reconstructions.

If the atoms are randomly distributed, the standard deviation associated with the measurement of the composition of the analyzed volume by APT is given by [13]:

$$\sigma = \sqrt{\frac{C(1-C)(1-Q)}{N}} \quad (1)$$

with C the measured composition, N the total number of atoms collected, and Q the detection efficiency ($Q \approx 0.5$). At the time of Palmière et al. study, 10 to 15 samples were needed to collect a total of 100,000 ions. Thus, the standard deviation associated with each experiment was very large, since it is related to the total number of collected ions (Eq. (1)): 22 ppm for a measured composition of 100 ppm and a total of 100,000 analyzed ions. During the last two decades, APT has considerably evolved in terms of analyzed volume size (total number of analyzed ions per sample) as well as in mass resolution [14,15]. This technique is nowadays capable of analyzing tens of millions of ions in a single sample. For such number of analyzed ions, the standard deviation associated with measurement becomes negligible. These evolutions open new perspectives for using APT as a quantitative tool for solid solution analysis.

In this article, APT was applied to determine the volume fraction of $(Ti_x,Nb_{1-x})C$ carbides of the order of 0.1% in an industrial Ti—Nb microalloyed steel. The characterization of the precipitation state within this steel by electron microscopy techniques is presented in [16]. The Nb and Ti concentration in austenite were measured after several heat treatments. Based on these measurements, the volume fraction of $(Ti_x,Nb_{1-x})C$ carbides was derived. Experimental data were then compared with Thermo-Calc [17] equilibrium calculations.

2. Material and methods

The bulk alloy composition was measured by inductively coupled plasma mass spectrometry (ICP-MS) and is given in Table 1.

The microstructure of the as-received state is mainly composed of granular bainite and is homogeneous (Fig. 1), no noticeable texture was observed. Several heat treatments were performed in the austenite stability domain between 1050°C and 1280°C, using parallelepiped samples of approximately 10 × 10 × 1 mm^3 machined from the as-received steel plate. Heat treatments are listed in Table 2. In order to avoid oxidation and decarburization, samples were placed in primary vacuum sealed quartz tube during heat treatments. The samples were directly inserted in horizontal radiative heating furnaces heated up to the target temperature, followed by water quenching. Martensitic microstructures were obtained after quenching.

The precipitation state of the initial condition and the heat treated

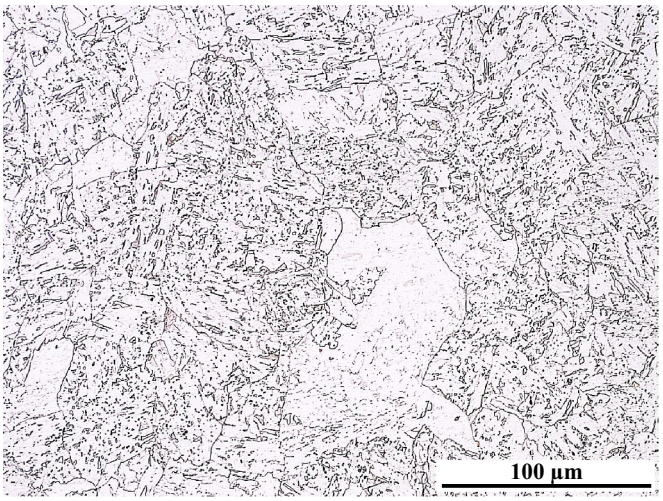

Fig. 1. Optical micrograph of the as-received steel microstructure, etched with Nital. An homogeneous granular bainite microstructure is observed, presenting no particular texture.

Table 2
Heat treatments performed.

Temperature (°C)	1050	1120	1200	1280
Time (min)	240	120	60	60

samples were investigated by means of electron microscopy. Special emphasis has been placed on the $(Ti_x,Nb_{1-x})C$ carbides, responsible for austenite grain growth control. Carbon extraction replicas were prepared and analyzed using a JEOL 2100 TEM operating at 200 kV and a ZEISS Supra 55VP FEG-SEM. To analyze larger precipitates that are not collected on carbon replicas, bulk samples were also investigated in SEM, after polishing down to 1 µm and nital etching. Both TEM and SEM were equipped with Oxford EDX analyzers with silicon drift detector (SDD). EDX measurements were employed to determine the relative contents of the metallic species such as Ti, Nb, and S. SEM-EDX measurements were conducted at 30 kV. Additionally, the crystallographic nature of precipitates was studied using selected area electron diffraction (SAED) on a JEOL 2010F TEM operating at 200 kV. The crystallography data used for indexing the SAED patterns are extracted from [18].

Atom probe tomography (APT) was applied to measure the austenite composition, with particular emphasis on Ti and Nb. The measurements were therefore performed on martensitic microstructures obtained by quenching after the heat treatments listed in Table 2. Due to the diffusion-less nature of its transformation mechanism, the composition of martensite is that of the parent austenite.

The specimen tips were prepared using a classical electro-polishing method. First, the tips were thinned using a solution of 75% acetic acid and 25% perchloric acid. Then, a final polishing was completed using a mixture of 2% perchloric acid in 98% 2 butoxyethanol at 15 V until separation of the rod into two pieces with a needle tip radius smaller than 50 nm. The experiments were carried out on a LEAP® 4000HR device from CAMECA under the following conditions: 20% pulse fraction, 50 K temperature and average detection rate of 0.3%. The

Table 1
ICP-MS composition (at.%) of the studied steel and mean APT composition (at.%) of all heat-treated samples. Ti, Nb, and C are not indicated in APT because they are involved in precipitates and vary depending on the heat treatment. N and S were not quantified by APT.

Element	Mn	Si	Al	Mo	V	Cr	Ti	Nb	C	N	S
ICP-MS	1.927	0.995	0.134	0.122	0.002	0.014	0.098	0.023	0.286	0.024	0.005
APT	1.689	1.060	0.133	0.116	0.002	0.013	–	–	–	–	–

reconstruction procedure was conducted using IVAS 3.6 software package. In order to get enough precision in the quantification of microalloying additions, several tens of millions of atoms were collected per heat treated condition.

In the experimental mass spectra generated, a convolution is observed between the peak of the main isotope of Ti ($^{48}Ti^{2+}$) and that of $(^{12}C\text{-}^{12}C)^{+}$ carbon molecular ions, around 24 Da. This was already observed by Thuvander et al. [19]. Therefore, the $^{48}Ti^{2+}$ peak, representing approximately 75% of the total Ti amount was not used for quantification of the Ti. In the same way, $^{49}Ti^{2+}$ and $^{50}Ti^{2+}$ peaks were not used due to convolutions with $(^{12}C\text{-}^{12}C\text{-}^{12}C\text{-}^{13}C)^{2+}$, $(^{12}C\text{-}^{13}C)^{+}$, and $^{50}Cr^{2+}$ peaks. Thus, the measurement of Ti in solid solution relied on the peaks of the two first isotopes ($^{46}Ti^{2+}$ and $^{47}Ti^{2+}$), representing 15% of the total Ti amount. The presented values were corrected according to natural isotopic ratios in order to estimate the actual Ti content.

For several millions of atoms, the standard deviation associated with the measurement of a composition by APT becomes negligible (Eq. (1)). Another source of error on this composition measurement can arise from APT very local nature, thus sensitive to possible heterogeneities in composition. For each heat-treated state, several samples were analyzed. The variation on composition measurement is referred to as the standard error of the mean ($\sigma_{\bar{x}}$) and is defined as the standard deviation divided by the number of observations n:

$$\sigma_{\bar{x}} = \sqrt{\frac{\sum_i (C_i - C_m)^2}{n}} \quad (2)$$

where C_m is the average composition measured, C_i the different individual compositions measured.

3. Results

3.1. Precipitation

In the as-received condition of the alloy, 4 different types of precipitates were identified, either on bulk samples or carbon replicas (Fig. 2): (Ti,Nb)N (a), complex precipitates composed of (Ti,Nb)N and MnS generally nucleated on an aluminum oxide inclusion (b), $Ti_4C_2S_2$ (c), and $(Ti_x,Nb_{1-x})C$ (d). Graux et al. [16] provides a more detailed characterization of the precipitation state of this alloy by electron microscopy techniques, EDX, and SAED.

Starting from this initial precipitated state, several reversion heat treatments were performed (Table 2). The precipitation state after each heat treatment was systematically investigated. The same four types of precipitates were also observed after heat treatments at 1050°C, 1120°C, and 1200°C. At 1280°C, only (Ti,Nb)N and MnS were observed on carbon replicas. A summary of the different precipitates found after each heat treatment is given in Table 3.

Table 3
Precipitates observed, total number of ions analyzed by APT, and austenite Ti/Nb solute content for each heat treatment performed. The standard error is calculated using Eq. (2).

Heat treatment	Temperature (°C)	1050	1120	1200	1280
	Time (min)	240	120	60	60
Precipitates observed (✓ = yes/✗ = no)	$(Ti_x,Nb_{1-x})C$	✓	✓	✓	✗
	(Ti,Nb)N	✓	✓	✓	✓
	$Ti_4C_2S_2$	✓	✓	✓	✗
	MnS	✓	✓	✓	✓
	Analyzed ions ($\cdot 10^6$)	17.9	60.2	100.4	47.5
Austenite composition	**Nb (at ppm)**	**4**	**61**	**155**	**201**
	Std error of the mean	1	6	11	22
	Ti (at ppm)	**141**	**290**	**412**	**531**
	Std error of the mean	15	7	33	67

Due to their small size (mean radius of 58 nm), $(Ti_x,Nb_{1-x})C$ exert a pinning pressure on austenite grain boundaries and are of particular interest for the control of austenite grain growth during heat treatments [16]. Depending on the heat treatment temperature, various amounts of $(Ti_x,Nb_{1-x})C$ are dissolved and released in solid solution. The other types of precipitates are often larger than 1 μm, which makes them ineffective for grain boundary pinning. The EDX analysis of $(Ti_x,Nb_{1-x})C$ gave a Ti/Nb ratio that was constant for each heat treatment, indicating that the $(Ti_x,Nb_{1-x})C$ composition remains stable over the temperature range studied. The Ti/Nb ratio is consistent with $(Ti_{0.80}Nb_{0.20})C$. Apart from very limited Mo amount (<1 at.%), no other metallic element were found in those precipitates. The large (Ti,Nb)N population only contains slights amounts of Nb. According to EDX analysis and assuming that they are pure nitrides, their Ti/Nb ratio is consistent with $(Ti_{0.95}, Nb_{0.05})N$. This population of precipitates is very stable, formed from the liquid state during casting. It is therefore reasonable to assume that $(Ti_{0.95}, Nb_{0.05})N$ do not significantly evolve for the considered heat treatments.

3.2. Austenite composition

APT was used to measure the austenite composition for each of the above-cited heat treatments. The total number of analyzed ions for each condition can be retrieved in Table 3. The amount of Ti and Nb in austenite increases with increasing heat treatment temperature, indicating the dissolution of $(Ti_x,Nb_{1-x})C$ precipitates. The heat treatments performed are long enough to reach equilibrium regarding the volume fraction of $(Ti_x,Nb_{1-x})C$ formed. Thus the austenite composition measurements give the solubility limits of $(Ti_x,Nb_{1-x})C$ at each temperature.

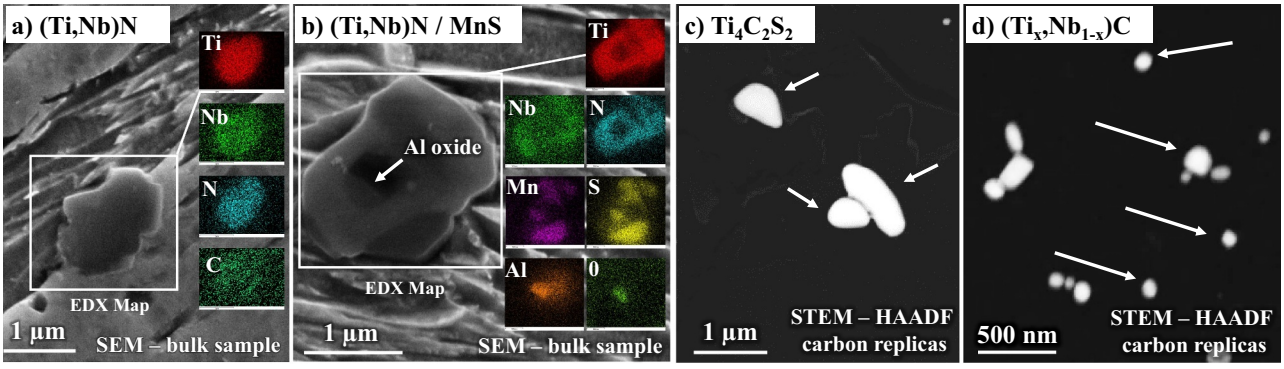

Fig. 2. SEM/TEM images of the four types of precipitates observed in the as-received condition of the alloy: (Ti,Nb)N (a), complex assemblies of (Ti,Nb)N and MnS nucleated on an aluminum oxide inclusion (b), $Ti_4C_2S_2$ (c), and $(Ti_x,Nb_{1-x})C$ (d). The $(Ti_x,Nb_{1-x})C$ (d) are the one of particular interest for austenite grain growth control [16].

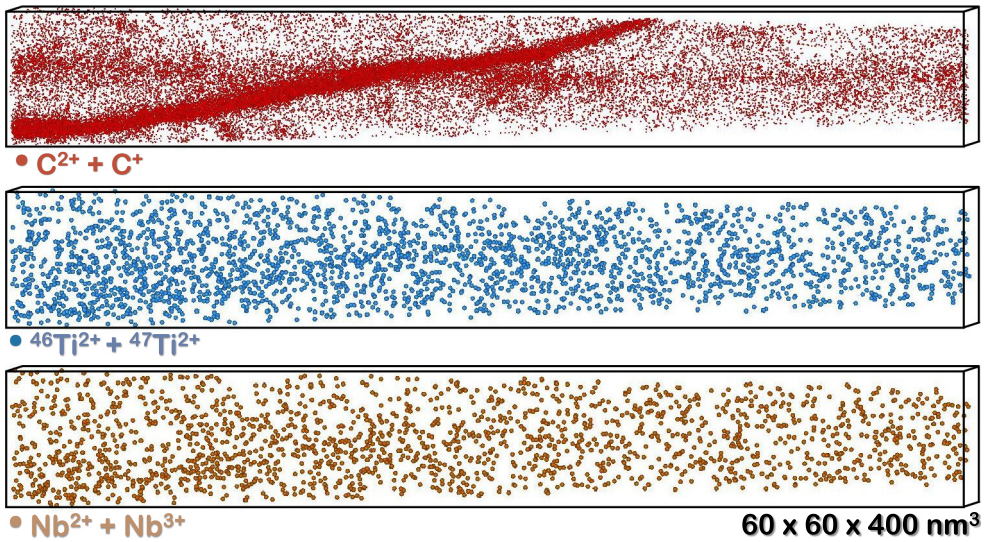

Fig. 3. Reconstructed atomic positions of a) carbon, b) niobium and c) titanium of an APT sample heat treated at 1200°C.

The analyzed volumes are up to 2 μm long, so that several martensite laths formed during quenching are analyzed. Fig. 3 displays the reconstructed positions of C, Nb, and Ti within a specimen heat treated at 1200°C, focusing on a martensite lath boundary. As expected for martensitic steels, a segregation of C is observed at lath boundaries. The distribution of Nb and Ti is more homogeneous throughout the sample. No precipitate was intercepted during analysis, therefore the whole tip composition measurement is representative of the matrix composition.

3.3. $(Ti_x,Nb_{1-x})C$ composition

A composition close to $(Ti_{0.80},Nb_{0.20})C$ was determined by EDX. This chemical content is inconsistent with the respective evolutions of Ti and Nb in solid solution measured by APT (see Table 3): since a difference in Nb in solid solution of about 200 ppm is observed between 1280°C and 1050°C, the difference of Ti content in solid solution between those two temperatures should be approximately 800 ppm (four times higher). A difference of approximately 400 ppm is found instead.

Therefore, an estimation of the composition of the $(Ti_x,Nb_{1-x})C$ population is proposed in this section, where x is the unknown to determine. The total amount of Ti and Nb available for the formation of $(Ti_x,Nb_{1-x})C$, respectively $X_{Ti}{}^0$ and $X_{Nb}{}^0$, are also estimated.

Since Nb evolution is only related to the $(Ti_x,Nb_{1-x})C$, the total amount of Nb available for the formation of $(Ti_x,Nb_{1-x})C$ is directly given by the APT measurement at 1280°C:

$$X^0_{Nb} = X^{SS}_{Nb,APT}(1280°C) = 201\,\text{ppm} \tag{3}$$

The Ti evolution from 1200°C to 1280°C is affected by the dissolution of both $(Ti_x,Nb_{1-x})C$ and $Ti_4C_2S_2$ (Fig. 4). Thus, the amount of Ti involved in both population has to be determined. Below 1200°C, it is however reasonable to assume that the evolution of Ti and Nb in solid solution is mainly related to the dissolution of $(Ti_x,Nb_{1-x})C$. The amount of $Ti_4C_2S_2$ at 1200°C and below is considered constant in the following calculations. Thus, the APT measurement at 1200°C is taken as the reference composition for the derivation of x and $X_{Ti}{}^0$.

At 1050 and 1120°C, the differences in Nb and Ti concentrations relative to the reference, ΔNb and ΔTi, are calculated (Fig. 5). Assuming that the evolution of the amounts of Ti and Nb in solid solution are only related to the $(Ti_x,Nb_{1-x})C$, the value of x can be estimated from the ratio $R = \Delta Ti/\Delta Nb$:

$$x = \frac{R}{1+R} \tag{4}$$

Although $R = 1.791$ and $R = 1.301$ are found at 1050°C and 1120°C respectively, R is considered to be constant over the temperature range studied as the composition of the $(Ti_x,Nb_{1-x})C$ precipitates was strictly identical from EDX measurement all over the considered temperature range. Therefore, the R value was chosen to be equal to the mean value, $\langle R\rangle = 1.546$. Thus, the precipitate composition coherent with the respective evolutions of Ti and Nb is $x = 0.61 \pm 0.04$.

The total amount of Ti available for the formation of $(Ti_x,Nb_{1-x})C$ is estimated using the mean R ratio, $\langle R\rangle$:

$$X^0_{Ti} = X^{SS}_{Ti,APT}(1200°C) + \langle R\rangle\cdot(X^0_{Nb} - X^{SS}_{Nb,APT}(1200°C)) = 483\,\text{ppm} \tag{5}$$

3.4. Estimation of $(Ti_x,Nb_{1-x})C$ volume fraction

The evolution of Nb solute content was used as the reference for the calculation of volume fraction. The volume fraction f_v was estimated from a mass balance, assuming that Nb atoms lie either in the solid solution or in the precipitates:

$$f_v = \frac{X^0_{Nb} - X^{SS}_{Nb}}{X^P_{Nb} - X^{SS}_{Nb}}\cdot\frac{v_P^{at}}{v_\gamma^{at}} \tag{6}$$

where $X_{Nb}{}^P$ is the atomic fraction of Nb within $(Ti_xNb_{1-x})C$, $X_{Nb}{}^{SS}$ is the atomic fraction of Nb in solid solution in austenite, $v_\gamma{}^{at}$ is the average atomic volume of austenite, and $v_P{}^{at}$ is the one of $(Ti_x,Nb_{1-x})C$. Here, $v_\gamma{}^{at} = 1.227 \times 10^{-29}\text{m}^3$ [20] and $v_P{}^{at}$ was calculated by a law of mixture between that of pure TiC and NbC:

$$v_P^{at} = x\cdot v_{TiC}^{at} + (1-x)\cdot v_{NbC}^{at} \tag{7}$$

with $v_{TiC}{}^{at} = 1.100 \times 10^{-29}\text{m}^3$, $v_{NbC}{}^{at} = 1.181 \times 10^{-29}\text{m}^3$ [20] and $x = 0.61$.

Neglecting the uncertainty on α_v, the uncertainty on the volume fraction, Δf_v, is given from the partial derivatives of f_v:

$$\Delta f_v = \left|\frac{\partial f_v}{\partial X^0_{Nb}}\right|\cdot\Delta X^0_{Nb} + \left|\frac{\partial f_v}{\partial X^{SS}_{Nb}}\right|\cdot\Delta X^{SS}_{Nb} + \left|\frac{\partial f_v}{\partial X^P_{Nb}}\right|\cdot\Delta X^P_{Nb} \tag{8}$$

with:

$$\frac{\partial f_v}{\partial X^0_{Nb}} = \frac{1}{\alpha_v\cdot(X^P_{Nb} - X^{SS}_{Nb})} \tag{9}$$

$$\frac{\partial f_v}{\partial X^{SS}_{Nb}} = \frac{X^P_{Nb} + X^0_{Nb}}{\alpha_v\cdot(X^P_{Nb} - X^{SS}_{Nb})^2} \tag{10}$$

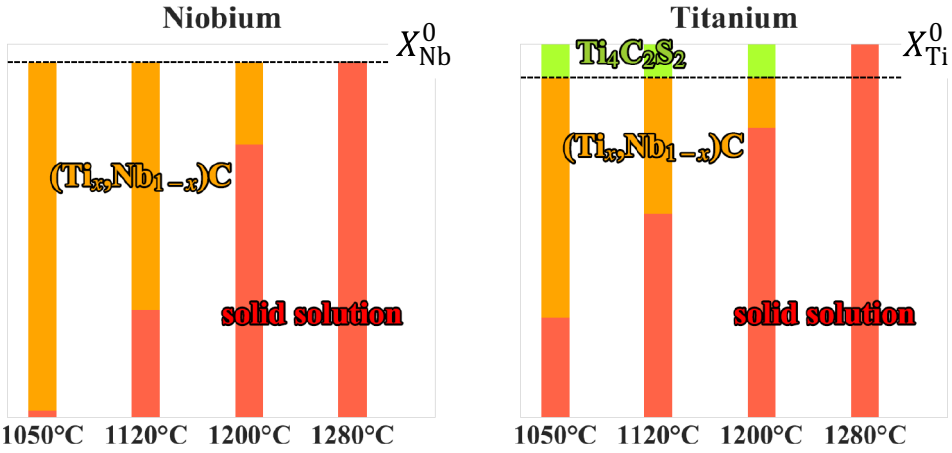

Fig. 4. Distribution of Nb and Ti for the investigated heat treated states, assuming that solute elements in (Ti,Nb)N remain trapped. Between 1280 and 1200°C, Nb evolution is only related to the formation of $(Ti_x,Nb_{1-x})C$ whereas Ti is affected by the formation of $(Ti_x,Nb_{1-x})C$ and $Ti_4C_2S_2$.

$$\frac{\partial f_v}{\partial X^P_{Nb}} = \frac{X^{SS}_{Nb} - X^0_{Nb}}{\alpha_v \cdot (X^P_{Nb} - X^{SS}_{Nb})^2} \quad (11)$$

The relative uncertainties on $X_{Nb}{}^{SS}$ are given in Table 3. The uncertainty on $\Delta X_{Nb}{}^0$ is equal to the one of $X_{Nb}{}^{SS}$ at 1280°C. Following the precipitate chemistry, $X_{Nb}{}^P$ is equal to $x/2$. Thus, the uncertainty on $X_{Nb}{}^P$ is estimated to 0.02 (0.04/2) according to the estimation of x presented in Section 3.3.

The calculated volume fraction after isothermal heat treatments can be retrieved in Table 4. As expected, the precipitated volume fraction increases as the heat treatment temperature decreases.

Table 4
Calculated volume fraction of $(Ti_x,Nb_{1-x})C$ from APT for each heat treatment performed.

Temperature (°C)	1050	1120	1200
Time (min)	240	120	60
Volume fraction (%) of $(Ti_x,Nb_{1-x})C$	0.109 ± 0.024	0.078 ± 0.023	0.026 ± 0.021

4. Discussion

In this work, the calculation of the volume fraction of $(Ti_x,Nb_{1-x})C$ relies on a mass balance between the total amount of microalloying elements available for $(Ti_x,Nb_{1-x})C$ precipitation ($X_{Ti}{}^0$ and $X_{Nb}{}^0$) and the actual amount of Ti and Nb in solid solution at a given temperature.

The measurement of solid solution Ti content was strongly hindered by the peak convolutions, so that only two isotopes representing 15% of the total Ti were used for the measurement. Since carbon will always be present in solid solution in microalloyed steels, this is a major disadvantage of this technique for measuring Ti solid solution contents. For this reason, the calculation of f_v was based on Nb, of which measurement suffers less limitations and uncertainties. Note that in a more general view, a limitation of the method is the ability to accurately determine the solute content of the matrix, even for very low content. This can be only performed if there are no peaks overlap in the mass spectrum, or if those peaks overlaps can be corrected.

Each individual composition measurement is affected by uncertainties linked to the analyzed volume and to the analysis of the mass spectrum. Due to the mass balance used, the calculation of f_v is not only affected by the uncertainties related to the matrix composition, $X_{Nb}{}^{SS}$, but also by those related to $X_{Nb}{}^0$. Therefore, the uncertainty in f_v is greater than that on the composition measurements. A poor estimate

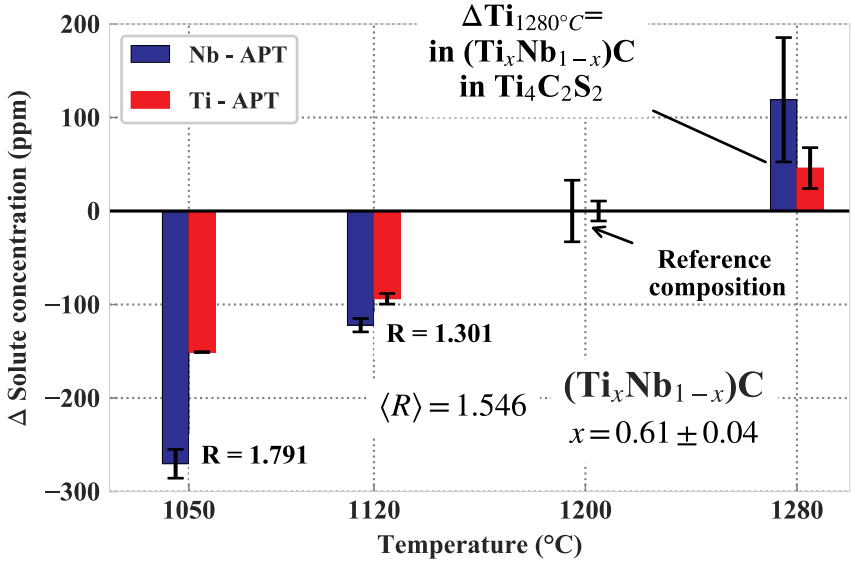

Fig. 5. Determination of x based on the respective evolution of Ti and Nb in solid solution below 1200°C. The total amount of Ti and Nb available for $(Ti_x,Nb_{1-x})C$ is deduced from the analysis.

Table 5
Calculation of the austenite composition considering the bulk ICP-MS composition and assuming that all N reacts with Ti and Nb to form $(Ti_{0.95}Nb_{0.05})N$.

Element	Ti	Nb	N	Others
Bulk ICP-MS (ppm)	984	230	237	Balance
Subtracting $(Ti_{0.95}Nb_{0.05})N$ (ppm)	754	218	0	Balance
APT at 1280°C	531	201	–	–

of X_{Nb}^0 can lead to completely erroneous estimates of f_v. Thus, as for any volume fraction determination technique based on mass balance, the proper determination of X_{Ti}^0 and X_{Nb}^0 is the most critical point for an accurate measurement. In this study, X_{Ti}^0 and X_{Nb}^0 are not equal to the total bulk alloy composition of the steel: a fraction of these elements are involved in other precipitates or may be segregated on defects such as grain boundaries.

At 1280°C, $(Ti_x,Nb_{1-x})C$ and $Ti_4C_2S_2$ are completely dissolved. Therefore, Ti and Nb can only be located in (Ti,Nb)N. Performing a simple mass balance, assuming that all N reacts with Ti to form pure $(Ti_{0.95}Nb_{0.05})N$ (according to EDX) leads to 754 ppm of Ti and 218 ppm of Nb remaining in solid solution (Table 5). The solid solution content measured by APT are significantly lower: 531 ppm of Ti and 201 ppm of Nb. A combination of two factors may explain this discrepancy. It is first possible that the (Ti,Nb)N nitrides are actually (Ti,Nb)(C,N) carbonitrides, which would increase the amount of Ti and Nb trapped in this population. Indeed, as seen in Fig. 2 a), it seems that slight amounts of carbon are present in these precipitates. It is also possible that a proportion of the total amount of Ti and Nb is trapped in austenite grain boundaries and not located within the austenite grains, where the APT samples are probably extracted. In order to avoid these difficulties, X_{Ti}^0 and X_{Nb}^0 are directly evaluated from APT measurements. Therefore, there is no need to locate all possible places where solute atoms may lie (segregated on defects and/or part of other precipitates). The direct measurement of the amount of solute atoms available for precipitation is much more precise than performing a mass balance from the bulk alloy composition.

A comparison of the atom probe measurements with equilibrium calculations is performed in Fig. 6. The measurements performed in this study are comparable with equilibrium calculations since recently published modelling results showed that $(Ti_x,Nb_{1-x})C$ reaches equilibrium volume fraction for the considered heat treatment times [16]. Equilibrium calculations were performed using TCFE8 database [20] on Thermo-Calc [17] software to predict the stability domain of the $(Ti_x,Nb_{1-x})C$. Calculations were run starting from the X_{Ti}^0 and X_{Nb}^0 determined with APT in Section 3.3. Sulfur and nitrogen were not considered in these calculations. The composition of other alloying elements are extracted from the ICP-MS bulk composition given in Table 1. Nb solid solution measurements by APT, on which volume fraction calculations are based, are in very good agreement with Thermo-Calc predictions.

On the other hand, the agreement regarding Ti is more questionable. Thermo-Calc predicted that the $(Ti_x,Nb_{1-x})C$ precipitates contain a greater proportion of titanium than what was estimated based on APT results: $x = 0.68$ for Thermo-Calc, against $x = 0.61 \pm 0.04$ based on solid solution measurements. The current method of estimating the measurement uncertainties, based on the standard error obtained on several experiment values, might not accurately reflect the intrinsic error done when measuring very low solid solution content. Thus, the measurement of the Ti content, which is made from two minor Ti peaks in the mass spectrum, may actually be affected by a greater uncertainty than that calculated.

Although the analyzed volumes by APT have largely increased these last two decades (typically around $60 \times 60 \times 1000\,nm^3$ for this study), APT measurements remain very local. By way of comparison, a few grams of material are analyzed with selective dissolution techniques, which represents a volume 10^{13} to 10^{14} times larger than those analyzed by APT. APT is thus much more sensitive to heterogeneities in matrix composition, due for example to macro segregations. Nevertheless, in the present case, the standard error observed on several samples of the same state remained limited, of the order of 10% of the measured composition. Moreover, the measurements are comparable with bulk ICP-MS for substitutional alloying elements, as observed in Table 1. The measurements therefore seem to remain fairly precise, with a limited uncertainty.

The results of this study show that APT is nowadays a reliable technique for measuring solute levels as low as a few tens of ppm, which is particularly useful for estimating the volume fraction of precipitates in microalloyed steels. The method used here is relevant and gives consistent results, comparable with equilibrium calculations. It is worth highlighting the complexity of the studied industrial material, which contains several types of precipitates and many alloying elements. For such complex precipitation states, the determination of $(Ti_x,Nb_{1-x})C$ volume fraction would have been rather complicated by TEM or SANS. Moreover, this type of analysis can be transposed to other steels with different compositions, as long as a special attention is paid to possible peak convolutions on the mass spectrum. The good resolution and stability of the technique also makes it a prime candidate for conducting more fundamental studies of solubility product

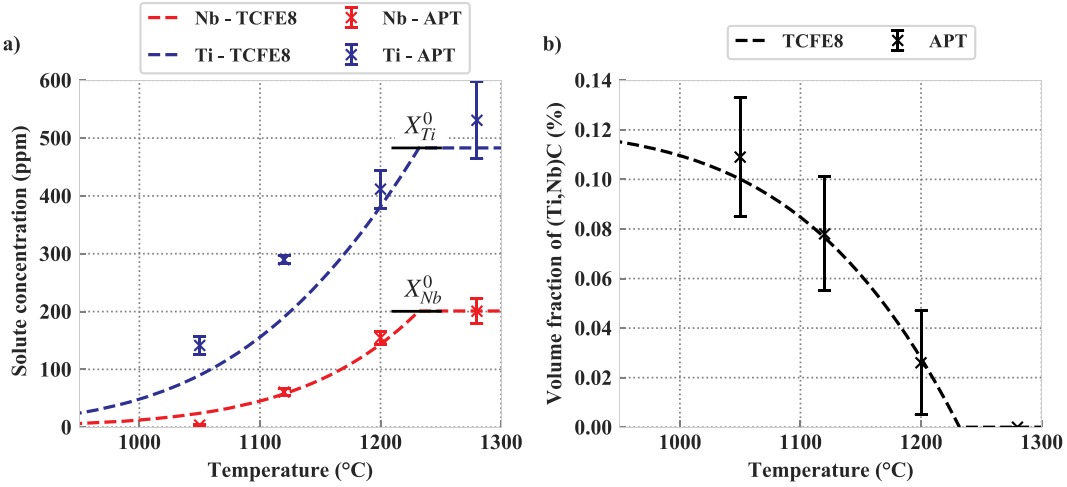

Fig. 6. Comparison of (a) composition of austenite and (b) $(Ti_x,Nb_{1-x})C$ volume fraction of precipitates determined by APT and by equilibrium calculations on Thermo-Calc.

determination. Note that such matrix composition measurements could be used to estimate a solubility product of $(Ti_x,Nb_{1-x})C$.

5. Conclusions

Atom probe analysis was applied to a Ti—Nb microalloyed steel, to follow the evolution of austenite solute composition in Ti and Nb as a function of temperature. The technique is sufficiently precise to measure very low solute contents of the order of a few tens of ppm, which is particularly suitable for microalloyed steels.

Knowing the matrix composition, and the precipitate composition, it is possible to estimate the volume fraction of precipitates by applying a simple mass balance calculation. The most critical issue is the correct estimation of the total amount of solute elements available for the formation of the considered precipitates, here $(Ti_x,Nb_{1-x})C$. This determination classically relies on the knowledge of the bulk alloy composition and the amount of atoms not involved in solid solution (usually involved in other precipitates). Direct atom probe tomography measurements of the amount of solute atoms available for $(Ti_x,Nb_{1-x})C$ precipitation avoid the difficult estimation of the amount of atoms possibly involved in many different places (primary precipitates, segregated on defects…).

Since the measurement of precipitate volume fraction in microalloyed steels is often tedious, it appears that atom probe is particularly suited for the measurement of the very low matrix compositions and precipitate volume fractions found in microalloyed steels. The technique also seems relevant to be used for the estimation of solubility products.

Declaration of competing interest

None.

Acknowledgments

The authors gratefully acknowledge the funding received from the European Commission, Research Fund for Coal and Steel, under grant agreement 709803 (NANOFORM). Thanks are due to the CLYM (www.clym.fr) for access to the 2010F microscope, and to Nicholas Blanchard for access and help on the JEOL 2100 microscope. This work was partly carried out owing to experimental GENESIS platform. GENESIS is supported by the Région Haute-Normandie, the Métropole Rouen Normandie, the CNRS via LABEX EMC, and the French National Research Agency as a part of the program “Investissements d'avenir” with the reference ANR-11-EQPX-0020.

Data availability

The raw/processed data will be made available on request.

References

[1] T. Gladman, D. Dulieu, Grain-Size Control in Steels, Metal Science 8 (1) (1974) 167–176.
[2] T. Gladman, Precipitation hardening in metals, Mater. Sci. Technol. 15 (1) (1999) 30–36.
[3] S.M. Allen, Foil thickness measurements from convergent-beam diffraction patterns, Philosophical Magazine A 43 (2) (1981) 325–335.
[4] M.F. Ashby, R. Ebeling, On the determination of the number, size, spacing, and volume fraction of spherical second-phase particles from extraction replicas, AIME Met Soc Trans 236 (10) (1966) 1396–1404.
[5] P. Maugis, S. Lanteri, D. Ravaine, P. Barges, M. Gouné, Y. Bi, M. Lamberigts, T. Siwecki, Development of methods for the characterisation and modelling of precipitation in steels, EUR, (20938) (2004) 1–230.
[6] D. Acevedo Reyes, M. Perez, S. Pecoraro, A. Vincent, T. Epicier, P. Dierickx, Vanadium carbide dissolution during austenitisation of a model microalloyed fecv steel, Materials Science Forum, volume 500, Trans Tech Publ, 2005, pp. 695–702.
[7] J. Lu, J.B. Wiskel, O. Omotoso, H. Henein, D.G. Ivey, Matrix dissolution techniques applied to extract and quantify precipitates from a microalloyed steel, Metall. Mater. Trans. A 42 (7) (2011) 1767–1784.
[8] F. De Geuser, A. Deschamps, Precipitate characterisation in metallic systems by small-angle x-ray or neutron scattering, Comptes Rendus Physique 13 (3) (2012) 246–256.
[9] A. Deschamps, F. De Geuser, Quantitative characterization of precipitate microstructures in metallic alloys using small-angle scattering, Metall. Mater. Trans. A 44 (1) (2013) 77–86.
[10] W. Rong, H.O. Andrén, H. Wisell, G.L. Dunlop, The role of alloy composition in the precipitation behaviour of high speed steels, Acta Metall. Mater. 40 (7) (1992) 1727–1738.
[11] M. Dumont, W. Lefebvre, B. Doisneau-Cottignies, A. Deschamps, Characterisation of the composition and volume fraction of η and η precipitates in an al–zn–mg alloy by a combination of atom probe, small-angle x-ray scattering and transmission electron microscopy, Acta Mater. 53 (10) (2005) 2881–2892.
[12] E.J. Palmiere, C.I. Garcia, A.J. De Ardo, Compositional and microstructural changes which attend reheating and grain coarsening in steels containing niobium, Metall. Mater. Trans. A 25 (2) (1994) 277–286.
[13] F. Danoix, G. Grancher, A. Bostel, D. Blavette, Standard deviations of composition measurements in atom probe analyses—part ii: 3D atom probe, Ultramicroscopy 107 (9) (2007) 739–743.
[14] M.K. Miller, T.F. Kelly, K. Rajan, S.P. Ringer, The future of atom probe tomography, Mater. Today 15 (4) (2012) 158–165.
[15] M.P. Moody, A. Vella, S.S.A. Gerstl, P.A.J. Bagot, Advances in atom probe tomography instrumentation: implications for materials research, MRS Bull. 41 (1) (2016) 40–45.
[16] A. Graux, S. Cazottes, D. De Castro, D. San Martín, C. Capdevila, J.M. Cabrera, S. Molas, S. Schreiber, D. Mirković, F. Danoix, et al., Precipitation and grain growth modelling in ti-nb microalloyed steels, Materialia (2019) 100233.
[17] J.-O. Andersson, Thomas Helander, Lars Höglund, Pingfang Shi, Bo Sundman, Thermo-Calc & DICTRA, computational tools for materials science, Calphad 26 (2) (2002) 273–312.
[18] S. Gražulis, D. Chateigner, R.T. Downs, A.F.T. Yokochi, M. Quirós, L. Lutterotti, E. Manakova, J. Butkus, P. Moeck, A. Le Bail, Crystallography open database – an open-access collection of crystal structures, J. Appl. Crystallogr. 42 (4) (2009) 726–729.
[19] M. Thuvander, J. Weidow, J. Angseryd, L.K.L. Falk, F. Liu, M. Sonestedt, K. Stiller, H.-O. Andrén, Quantitative atom probe analysis of carbides, Ultramicroscopy 111 (6) (2011) 604–608.
[20] Thermo-calc Software TCFE8 Steels/Fe-alloys Database (accessed July 30, 2018).